1	Title: Models of knot and stem development in black spruce trees indicate a shift in allocation
2	priority to branches when growth is limited
3	
4	
5	
6	Authors: Emmanuel Duchateau <sup>1</sup> , David Auty <sup>1,2</sup> , Frédéric Mothe <sup>3</sup> , Fleur Longuetaud <sup>3</sup> , Chhun-
7	Huor Ung <sup>4</sup> , Alexis Achim <sup>1*</sup>
8	
9	
10	
11	
12	<sup>1</sup> Renewable Materials Research Centre, Université Laval, 2425 rue de la Terrasse,
13	Québec G1V 0A6, QC, Canada
14	<sup>2</sup> Current address: Northern Arizona University, 200 East Pine Knoll Drive, Flagstaff, AZ
15	86011-5018
16	<sup>3</sup> AgroParisTech, UMR1092 LERFoB, 54000 Nancy, France
17	<sup>4</sup> Natural Resources Canada, Canadian Wood Fibre Centre, Laurentian Forestry Centre, 1055 du
18	P.E.P.S., P.O. Box 3800, Sainte-Foy, Quebec G1V 4C7
19	
20	
21	
22	*For correspondence. Email: <u>alexis.achim@sbf.ulaval.ca</u>
23	

# **Abstract**

The branch autonomy principle, which states that the growth of individual branches can be
predicted from their morphology and position in the forest canopy irrespective of the
characteristics of the tree, has been used to simplify models of branch growth in trees. However,
observed changes in allocation priority within trees towards branches growing in light-favoured
conditions, referred to as 'Milton's Law of resource availability and allocation', have raised
questions about the applicability of the branch autonomy principle. We present models linking
knot ontogeny to the secondary growth of the main stem in black spruce (Picea mariana (Mill.)
B.S.P.), which were used to assess the patterns of assimilate allocation over time, both within
and between trees. Data describing the annual radial growth of 445 stem rings and the three-
dimensional shape of 5377 knots were extracted from optical scans and X-ray computed
tomography images taken along the stems of 10 trees. Total knot to stem area increment ratios
(KSR) were calculated for each year of growth, and statistical models were developed to
describe the annual development of knot diameter and curvature as a function of stem radial
increment, total tree height, stem diameter, and the position of knots along an annual growth
unit. KSR varied as a function of tree age and of the height to diameter ratio of the stem, a
variable indicative of the competitive status of the tree. Simulations of the development of an
individual knot showed that an increase in the stem radial growth rate was associated with an
increase in the initial growth of the knot, but also with a shorter lifespan. Our results provide
support for 'Milton's Law', since they indicate that allocation priority is given to locations where
the potential return is the highest. The developed models provided realistic simulations of knot
morphology within trees, which could be integrated into a functional-structural model of tree
growth and above-ground resource partitioning.

### Introduction

1

Models of carbon assimilate allocation in trees generally consider branches to be part of either the woody shoot or the crown (Landsberg and Waring 1997; Mathieu et al. 2009). However, considering branch xylem as a separate sink can extend the practical applicability of functional-

5 structural tree models (FSTMs; Sievänen et al. 2000) to include wood properties considerations.

6 Knots are formed when branches are occluded by growing tree stems, and exert a strong

influence on the end-use characteristics of wood products (Buksnowitz et al. 2010). Knots affect

8 both visual and mechanical properties, and consequently lumber value (Dinwoodie 2000).

9 Therefore, silviculturists need tools to understand the trade-offs between stem radial growth and

branch size (Weiskittel et al. 2007; Hein et al. 2008), while among wood processors there is

increasing interest in optimizing lumber production by accounting for the location and size of

knots within logs (Lemieux et al. 2002; Moberg and Nordmark 2006).

13

23

10

11

7

14 Knot formation is driven by complex spatiotemporal interactions between a tree and its 15 environment. Thus, knowledge of the biological processes that regulate assimilate partitioning in 16 trees could improve models of branch growth. The branch autonomy principle (Van der Wal 17 1985; Sprugel and Hinckley 1988) has been used in some FSTMs to simplify the modelling 18 process (Bosc 2000; Kull and Tulva 2000). The branch autonomy principle states that the growth 19 of individual branches can be predicted from their morphology and position in the forest canopy, 20 irrespective of tree characteristics. Models that incorporate this principle can also predict 21 mortality based on the growing space (Mitchell 1975) or the amount of light (Nikinmaa and Hari 22 1990) available to individual branches. However, there is an important limitation to this

principle. By comparing the height of the lower limit of the living crown in trees of different

1 sizes, Sprugel (2002) showed that branches on supressed trees were more likely to survive and 2 grow than the equivalent branches on dominant trees. This implied shift in allocation priority 3 within trees towards branches in light-favoured positions, referred to as 'Milton's Law of 4 resource availability and allocation' (Sprugel 2002), suggests that assimilates are invested where 5 the potential return is highest. This is consistent with the results of Nikinmaa et al. (2003), who 6 obtained improved predictions of crown development when considering both the position and the light environment of branches. However, experimental confirmation of Milton's Law is 7 8 generally restricted to static assessments of the location of the crown base in even-aged forest 9 stands (Valentine et al. 2013). 10 Branch ontogeny can be studied in long-term experiments (Pretzsch 2005), but repeated 11 12 measurements on the same trees are time-consuming and costly. One solution to this problem is 13 to use empirical branch distribution models to simulate the temporal development of tree and 14 branch growth using cross-sectional data i.e. observations of the number, location and size of 15 branches made on trees of different ages (Colin and Houllier 1991; Mäkinen and Mäkelä 2003; 16 Achim et al. 2006; Weiskittel et al. 2007). However, the simplicity of the approach comes at the 17 expense of reduced accuracy for some branch measurements (Duchateau et al. 2013a). More 18 recently, non-destructive techniques for rapidly generating high-resolution data have been 19 developed, such as infrared imaging, optical scanning, magnetic resonance imaging (MRI), and 20 computed tomography (CT) using X-rays or gamma rays (Moberg 2001; Longuetaud et al. 2012; 21 Dutilleul et al. 2014). These innovations allow the use of internal data to simultaneously

23

22

reconstruct stem and knot growth over time.

14

15

1	In this study we present mod	els linking knot	ontogeny to the	secondary growth o	of the main stem
---	------------------------------	------------------	-----------------	--------------------	------------------

- 2 in black spruce (*Picea mariana* (Mill.) B.S.P.), a dominant species in the North American boreal
- 3 forest. We used data from high-resolution CT scans of tree stems to reconstruct the history of
- 4 both stem and knot development, with the aim of developing models that would apply in an
- 5 FSTM framework. First, we tested the hypothesis that the ratio of branch to stem growth was
- 6 dependent on stem characteristics indicative of the competitive status of the tree. We then
- 7 developed statistical models for predicting the evolution of individual knot diameter and
- 8 curvature using a series of predictors related to the position in the tree, stem radial growth, and
- 9 other general stem characteristics. This allowed us to test 'Milton's Law' using longitudinal data
- i.e. repeated measurements of branch and stem growth over time. This approach allowed us to
- make detailed simulations of knot development while considering the variation in assimilate
- 12 partitioning between trees.

# Materials and methods

## Tree sampling

- Sample trees were collected from seven naturally-regenerated, unmanaged forest stands in the
- 17 North-Shore region of Quebec, Canada. All sampling locations were part of a network of sites
- established to study the growth of spruce-moss forests after fire (Barrette et al. 2013; Torquato et
- al. 2014; Ward et al. 2014). At the time these plots were established, efforts were made to
- 20 maintain site characteristics (i.e. surface deposit, topographic position, exposure and soil
- 21 drainage) as constant as possible and representative of mesic conditions (Ward et al. 2014).

- 1 Because CT-Scanning is costly and the associated data processing time-consuming, we worked
- 2 with a limited number of sample trees. In each of the seven stands, two trees were randomly
- 3 selected for destructive sampling. However, four trees were omitted from the analysis due to
- 4 missing discs and the presence of wood decay. Of the ten trees in our final sample, eight came
- 5 from even-aged plots that had regenerated after fires dating back to between 66 and 152 years
- 6 (Bouchard et al. 2008). Two more trees (T09 and T10) were selected from one uneven-aged plot
- 7 where the time since the last stand-replacing fire exceeded 200 years. The sample trees had a
- 8 wide range of ages, crown size and stem dimensions (Table 1).

10

### Annual knot data

- After felling, each tree was cut into 2.5-m logs, giving a total of 41 logs that were then
- 12 transported to the Institut National de la Recherche Scientifique in Quebec City and scanned
- using a Somatom Sensation 64 CT scanner (Siemens Medical Solutions USA, Inc., Malvern,
- 14 PA). Each log was scanned at 2-mm intervals along its longitudinal axis with a 2-mm-wide X-
- 15 ray beam (120 kV-50 mA), so that the scanned segments were contiguous. The pixel size was
- 16  $0.35 \text{ mm} \times 0.35 \text{ mm}$  in the transverse direction.

- 18 Knot geometry was extracted using the ImageJ 1.44 free software (Abramoff et al. 2004), with a
- 19 Java plug-in ('Gourmand', version 1.01) developed at INRA, Nancy, France (Longuetaud et al.
- 20 2012). On successive images, the edges of each knot were manually delineated with a series of
- 21 points (Fig. 1A). A second purpose-built plug-in named 'BIL3D' (Colin et al. 2010) was
- 22 developed to extract the position and 3D geometry of each knot using the Cartesian coordinates
- of each point (Fig. 1B). The cross section of each knot from its point of origin to the bark of the

- 1 stem was represented by fitting successive circles in the longitudinal-tangential plane to the
- 2 points located manually at the tangential limits of the knots on successive CT images. In a
- database, the diameter (D) of each circle was recorded, as well as the distance from the stem's
- 4 pith (1) and position of its geometrical centre along the longitudinal stem axis (Z, referred to as
- 5 the 'vertical position'). This way, we obtained a representation of the geometric profiles of 5377
- 6 knots. A more detailed description of the knot reconstruction method was presented by
- 7 Duchateau et al. (2013*a*).

- 9 Knot development for each successive year of growth (t) was reconstructed using the diameter
- 10  $(D_t)$  and vertical position  $(Z_t)$ . To avoid local irregularities associated with the manual extraction
- of knot boundaries on the CT images, and to obtain a parametric description of each knot that
- was dependent on the radial position within the stem, smoothed knot profiles were obtained by
- fitting the same nonlinear model to both series of  $D_t$  and  $Z_t$  measurements. This was based on a
- Weibull equation with an additional linear term:

15

16 
$$y_t = \alpha \left(1 - e^{\left(-\beta \left(\frac{l}{R_{max} - l}\right)\right)}\right) + \mu \cdot l$$
  $(0 \le l \le R_{max})$ 

- where  $y_t$  represents either the  $D_t$  or  $Z_t$  values (mm), l is the position along the x-axis (mm),  $R_{max}$
- is the total length (mm) of the knot along the x-axis and  $\alpha$ ,  $\beta$  and  $\mu$  are parameters to be
- 19 estimated empirically. This model was selected because it can accurately describe a wide variety
- of knot shapes (Duchateau et al. 2013a).

- The functions were fitted to each knot independently using the *nls* function of the *nlme* library in
- 23 the R statistical programming environment (R Core Team, 2014). The models for both D<sub>t</sub> and Z<sub>t</sub>

- 1 converged for 95% of the knots in the database. Visual examination revealed that non-
- 2 convergent knots were generally small and sinuous. Indeed, convergent knots represented 98%
- 3 of the total volume of knots in the entire dataset, which we considered representative of the full
- 4 history of knot growth in our sample trees.

6

### Annual ring data from the main stem

- 7 Annual ring data from the main stem were difficult to obtain from the CT images due to factors
- 8 such as narrow rings and the higher moisture content of the sapwood. One-cm-thick discs were
- 9 hence cut from the ends of each log to reconstruct the growth history of the stems. Discs were
- optically scanned and annual ring boundaries were delineated in the four cardinal radial
- directions using image analysis software (WinDENDRO<sup>TM</sup>; Régent Instruments, Quebec City,
- 12 2005; Guay et al. 1992).

13

- 14 To link annual changes in knot geometry with stem radial increments, we estimate the latter at
- 15 the position of each knot. In each cardinal direction, a linear interpolation was made between the
- widths of each matching ring from both ends of each log (Fig. 2A). For rings present near the
- 17 pith of the lower disc but absent from the upper disc, we used the mean linear interpolation
- 18 coefficient of the first five complete rings. This way, we obtained estimates of annual ring widths
- at any height along the stem in the four main cardinal directions.

- 21 To reconstruct stem growth in the azimuthal direction of each knot (Fig. 2B), a second
- 22 interpolation was made from the two surrounding cardinal directions for which we had
- 23 measurements. In this case we used a weighted average of the two known ring width series

- located on each side of the knot. We defined  $\alpha_r$  as the azimuth angle between a knot and one of
- the two cardinal directions on each side. The weighting factor was calculated as  $(90-\alpha_r)/90$ ,
- 3 which approached a value of 1 if the knot orientation was close to one of the cardinal directions.
- 4 Due to irregularities in stem shape, the resulting series of stem rings associated with a given knot
- 5 did not end in the same exact location as the knot-stem interface was located on the CT images.
- 6 Therefore, a small correction constant was added (or subtracted) to each ring in the series to
- 7 ensure that both matched exactly.

- 9 In a final step in the knot and stem growth reconstruction process, we traced back the annual
- limits of primary growth. Each annual elongation of the shoot was defined as a growth unit
- 11 (GU). Like other conifers, black spruce produces several nodal and internodal branches within a
- growth unit. Nodal branches are those forming a whorl at the top of a GU (Achim et al. 2006,
- 13 Auty et al. 2012). Botanically, the branches of conifers do not technically originate from the
- same vertical position, these are referred to as 'pseudo-whorls' (Fisher and Honda 1979).
- 15 However, this distinction was not apparent at the resolution of our CT-scanning measurements.
- 16 Therefore, we summed the basal areas of all branches that originated from the same CT image,
- 17 which facilitated the identification of pseudo-whorls of branches that were used as the limits of
- annual GUs. To avoid large errors, we ensured that the number of GUs matched the difference in
- 19 the number of annual rings measured at both ends of each log. A more detailed description of the
- 20 growth unit identification method is presented in Duchateau et al. (2013b).

- 22 Once we had obtained a full description of both the knots and stem shape, a final step was to
- obtain the annual increments in knot diameter ( $\Delta D_t$ ) and vertical position ( $\Delta Z_t$ ). These were

- 1 computed using the intersection points between stem rings and knots. The diameter of each knot
- 2 was measured perpendicular to its central axis at each intersection point (Fig. 2)

4

### Model development

5 Tree-level models

- 6 To examine the variation in biomass allocation between the stem and branches over time, the
- 7 ratio of knot to stem growth (KSR<sub>i,t</sub>, dimensionless) was calculated, for each year of growth (t),
- 8 as the sum of all knot area increments at the surface of the stem divided by the annual basal area
- 9 increment of the stem at 1.3 m. This process was repeated for all years with complete growth
- data along the stem. When knots had reached a constant or decreasing diameter they were
- 11 considered to be dead.

12

- To assess the variation of KSR<sub>i,t</sub> through the life of the tree, we developed a linear mixed-effects
- model (Pinheiro and Bates 2009) describing its evolution as a function of tree height-diameter
- ratio and tree age. To assess the effect of within stand competition on KSR<sub>i,t</sub>, the ratio (HD<sub>i,t</sub>,
- 16 m/cm) between tree height  $(H_{i,t})$  and its diameter at breast height  $(DBH_{i,t})$ , measured at 1.3 m)
- was used as a surrogate for the competitive status of the subject trees at a given age. This ratio is
- 18 useful because inter-tree spacing is known to strongly affect crown development and hence the
- radial growth of the stem, whereas it has much less effect on height growth (Weiskittel et al.
- 20 2011). Since values of KSR<sub>i,t</sub> were continuous and non-negative, it was modelled as a gamma
- 21 distribution with a log-link:

23 
$$ln(KSR_{it}) = a_1 + a_2 \cdot HD_{i,t} + a_3 \cdot Age_{i,t} + \delta_i$$
 (2)

- 1 where ln(KSR<sub>i,t</sub>) is the natural logarithm of the knot to stem ratio in a given year, Age<sub>i,t</sub> is the age
- of the tree (years),  $a_1$ ,  $a_2$ ,  $a_3$  are the model parameters and  $\delta_i$  is the random effect for each tree (i).

- 4 Next, we examined the effect of KSR<sub>it</sub> on the number of new branches produced in a given year
- 5 by fitting a Poisson regression model, with a log-link, describing the number of new branches
- 6 per stem as a function of KSR<sub>it</sub>, tree age and their interaction:

7

- $8 \quad ln(NBR_{it}) = b_1 + b_2 \cdot KSR_{it} + b_3 \cdot Age_{it} + b_4 \cdot KSR_{it} \cdot Age_{it} + \delta_i$ (3)
- 9 where ln(NBR<sub>it</sub>) is the natural logarithm of the number of new branches per stem in a given year,
- $b_1$ ,  $b_2$ ,  $b_3$ ,  $b_4$  are the model parameters, and all other variables are as previously defined.

- The models presented in equations 2 and 3 were fitted using the *glmer* function in the *lme4*
- library (Bates et al. 2014) of the R statistical programming environment (R Core Team 2014).
- 14 Tree-level random effects were included to account for the hierarchical structure of the data
- 15 (Pinheiro and Bates 2009). In model fitting, we began by screening all potential tree-level
- 16 explanatory variables and biologically plausible interaction terms. Variables were selected after
- 17 calculating the variance inflation factors (VIF), to address any potential multicollinearity issues
- 18 (O'brien 2007). Variables that were highly correlated (VIF >4) were excluded from the models.
- 19 Variable selection was achieved using a backwards elimination process and model selection was
- 20 based on Akaike's information criterion (AIC) (Akaike 1974). Chi-squared-based likelihood
- 21 ratio tests were used to evaluate the significance of terms that were successively dropped from
- 22 the model. In the absence of a significant difference (p>0.05), the simplest model was retained.
- 23 Parameter estimates were obtained using the maximum likelihood method.

2 Individual knot models

- 3 Next, statistical models were developed to describe the temporal evolution of the morphology of
- 4 individual knots using annual ring- and tree-level characteristics as independent variables.
- 5 Initially, we attempted to fit a single model describing both vertical position  $(Z_{i,j,t})$  and knot
- 6 diameter  $(D_{i,j,l})$  simultaneously, thereby reconstructing the entire knot in a single step. However,
- 7 this led to an underestimation of knot diameter in the first years of growth that carried over for
- 8 the entire knot profile. Therefore, separate models were developed for each separate component.
- 9 Also, the models describing each component over time were divided into sections to facilitate the
- 10 fitting process. Individual knot diameter and curvature models were fitted to the data from a
- 11 random selection of 75% of the total population of knots, while the remaining data were used for
- 12 model evaluation.

13

14

#### Knot diameter model

- We observed relatively consistent patterns in the diameter development of the knots. There was a
- 16 rapid increase in diameter increment in the first three years of knot growth, followed by a
- 17 gradual decline until branch death (Fig. 4A). On average, branch increments reached zero at
- around year 25. We hence divided each diameter profile into three sections: 1) the initiation
- 19 section (years 0 to 3), 2) the growth section (years 4 to 25) and 3) the stable or declining section
- 20 (years > 25). In the initiation section, because  $\Delta D_{i,j,t}$  values did not follow a Gaussian
- distribution,  $D_{i,j,t}$  was modelled directly. In the remaining two sections  $\Delta D_{i,j,t}$  was used as the
- 22 response variable.

- 1 Knot characteristics at time t-1 were used to make predictions at time t. This ensured a smooth
- 2 transition between the different sections of the model. After the variable selection process, the
- 3 general form of the knot diameter model could be expressed as:

- $5 \qquad \Delta D_{i,j,t} \ or \ D_{i,j,t} = c_1 + c_2 \cdot \Delta D_{i,j,(t-1)} + c_3 \cdot D_{i,j,t-1} + c_4 \cdot GU_{pos \ i,j} + c_5 * l_{i,j,t} + c_6 \cdot RW_{i,j,t} + c_7 * l_{i,j,t} + c_6 \cdot RW_{i,j,t} + c_7 * l_{i,j,t} + c_8 \cdot RW_{i,j,t} + c$
- 6  $HD_{i,t} + c_8 \cdot Age_{i,t} + c_9 \cdot DBH_{i,t} + c_{10} \cdot H_{i,j} + \delta_{i,j} + \varepsilon$  (4)
- $\label{eq:continuous} 7 \qquad \text{where } GU_{pos\,i,j} \text{ is the relative position of the knot initiation point } along \text{ the } GU \text{ (varies from 0 at } in the continuous of the knot initiation point } in the continuous of the knot initiation point } in the continuous of the knot initiation point } in the continuous of the knot initiation point } in the continuous of the knot initiation point } in the continuous of the knot initiation point } in the continuous of the knot initiation point } in the continuous of the knot initiation point } in the continuous of the knot initiation point } in the continuous of the knot initiation point } in the continuous of the knot initiation point } in the continuous of the knot initiation point } in the continuous of the knot initiation point } in the continuous of the knot initiation point } in the continuous of the knot initiation point } in the continuous of the knot initiation point } in the continuous of the knot initiation point } in the continuous of the knot initiation point } in the continuous of the knot initiation point } in the continuous of the knot initiation for the kno$
- 8 the base to 1 at the stem apex), RW<sub>i,j,t</sub> is the ring width of the stem at the location of the knot in
- 9 year t,  $\delta_{i,j}$  are the tree- and knot-level random effects and  $\varepsilon$  is the residual error. All other
- 10 variables are as previously defined.

## 11 Knot curvature model

- 12 The average annual variation of  $\Delta Z_{i,j,t}$  was typically positive until approximately ring 40. After
- this point the vertical position stabilized, before decreasing after ring 60 (Fig 4B). The knot
- vertical position profiles were therefore separated into two sections delineated at ring number 50.
- 15 Characteristics of the knots in year *t*-1 were also included in this model, thus ensuring a smooth
- 16 transition between the sections. Various combinations of the explanatory variables were used in
- each section of the model. The general form of the knot diameter model was expressed as:

18

- 19  $\Delta Z_{i,j,t} = d_1 + d_2 \cdot D_{i,j,(t-1)} + d_3 \cdot \Delta Z_{i,j,(t-1)} + d_4 * \cdot l_{i,j,t} + d_5 \cdot RW_{i,j,t} + d_6 \cdot GU_{pos\ i,j} + d_7 \cdot HD_{i,t} + d_8 \cdot GU_{pos\ i,j} + d_7 \cdot HD_{i,t} + d_8 \cdot GU_{pos\ i,j} + d_8 \cdot GU_{$
- 20  $d_8 \cdot Age_{i,t} + d_9 \cdot DBH_{i,t} + \delta_{i,j} + \varepsilon$  (5)
- 21 where all variables are as previously defined. See Table 2 or a full description of all variable
- 22 names used in the models.

- 1 These models were fitted using functions contained in the *nlme* library of the R statistical
- 2 programming environment (R Core Team 2014). A power variance function of annual ring
- 3 number from the pith at the level of each knot (RN) was included to account for
- 4 heteroscedasticity in the model residuals. In addition, a continuous first-order auto-regressive
- 5 term (AR1) was added to account for autocorrelation between successive measurements. The
- 6 model fitting process started by including a full set of potential ring-, knot- or tree-level
- 7 explanatory variables and model selection was performed using the same backwards elimination
- 8 procedure as described in the section on tree-level models.

10 Simulations

- To analyse the influence of tree growth and competitive status on knot development, we
- reconstructed a single knot at 6.1 m using the predictions from equations 3 and 4 and the stem
- and growth characteristics of tree T10. Then, while keeping tree height constant, we increased
- the annual ring increments by 50%. The diameter and vertical profiles of the original knot were
- then recalculated. The process was repeated by decreasing the annual stem increments of the
- same tree by 50% of their actual values and again predicting knot morphology.

17

- 18 In a second simulation, all knots from a 1.5-m section starting at a height of 2.5 m in tree T4
- were simulated using equations 3 and 4 and compared to the real knots, as extracted from the CT
- 20 images. For this simulation we used the known insertion points along the stem and azimuthal
- 21 orientation of each knot. Where appropriate, the year at which a knot was observed to be
- 22 completely occluded by the growing stem was used as the end-point of the simulation.

# Results

1

2

5

7

8

9

10

### Tree-level models

3 The knot to stem increment ratio (KSR<sub>t</sub>) varied considerably with tree age. On average, KSR<sub>t</sub>

4 was higher when trees were young and decreased rapidly in the first few years, before stabilizing

(Fig. 5). The rate of the initial decrease varied among trees. Values of KSR<sub>t</sub> greater than 1

indicated that, in a given year, the total knot basal area increment exceeded that of the stem. In

addition to the negative relationship with tree age, KSR<sub>t</sub> ratio was positively related to HD<sub>t</sub>, such

that more slender trees allocated relatively more biomass to their branches than to the main stem

(Fig. 6). Furthermore, in a given year, the predicted number of new branches produced was

greater in trees with higher KSR<sub>t</sub> values, but the effect of KSR<sub>t</sub> decreased with increasing tree

11 age (equation 3; Table 3).

12

14

15

16

17

13 In some trees, KSR values showed large interannual fluctuations from the general trend (Fig. 5).

The 3D reconstructions of the stem and knots for two of these trees showed large deviations of

the pith of the main stem, likely a result of leader loss or stem damage. While one of these trees

retained apical dominance in a single leader (T01), the other produced a fork (T09; Fig. 7). The

model produced a good fit to all trees except tree T03, although visual examination of the 3D

reconstruction of this stem revealed no obvious explanation for the lack of fit.

19

#### **Knot-level models**

- 2 Table 4 shows the fixed effects parameter estimates and standard errors for each section of the
- 3 final knot diameter model (equation 4). To evaluate the model, knot diameter profiles were
- 4 predicted and compared to observations in the evaluation dataset. Plots of the raw residuals
- 5 (observed minus predicted values) showed that, on average, knot diameter was slightly
- 6 underestimated in the middle section of the knot profiles, but overall the model was unbiased
- 7 (Fig 8A). The absolute value of 50% of the residuals was less than 2.6 mm along the pith-to-bark
- 8 profiles, while the absolute value of 90% of the residuals was less than 9.7 mm. The mean
- 9 absolute error was 0.031 and the root mean square error (RMSE) 0.054.

10

1

- 11 Table 5 shows the fixed effects parameter estimates and associated standard errors for each
- section of the final model of knot vertical position (equation 5). Again, predictions of knot
- vertical profiles were compared to observations in the evaluation dataset. On average, the model
- was unbiased along the knot profile up to ring 75, with a slight overestimation beyond this point
- 15 (Fig. 8B). The absolute value of 50% of the residuals was less than 11.9 mm along the entire
- pith-to-bark profiles, while the absolute value of 90% of the residuals was less than 36.7 mm.
- 17 The mean absolute error for this model was 0.118 and the root mean square error (RMSE) 0.189.

18

19

#### **Simulations**

- When we used the dimensions and growth of a real tree (T10) to simulate knot growth, the
- 21 diameter increments in the early years of knot development were positively related to the radial
- 22 growth of the main stem. However, knot longevity was reduced when the radial growth was

- 1 artificially increased (and thus the HD ratio decreased). Knot growth ceased at ring 19 for the
- 2 elevated growth scenario, but it was maintained along its entire profile (47 years) when stem
- 3 growth was reduced (Fig. 9). In the real growth scenario, knot diameter increments began to
- 4 decline around ring 25. Tree HD ratio also had a significant effect in the first section of the knot
- 5 curvature model, although the effect was only apparent in the lower stem (not shown).

- 7 In the second simulation we reconstructed all knots in a 1.5-m section of tree T04. This showed
- 8 that although the diameter of larger knots was slightly underestimated, the models generally
- 9 produced accurate simulations of the diameter and shape of real knots. However, the models
- produced less variation in knot insertion angle than was observed in reality (Fig. 10), which
- would likely explain the larger residuals of the vertical position model.

12

13

14

# **Discussion**

### **Resource allocation**

- 15 This study provides further support to the idea that allocation of above-ground carbon assimilates
- in trees is directed towards locations where the potential return is the highest (Sprugel 2002). To
- 17 maintain a favourable position in the canopy, trees subjected to high levels of competition
- prioritize height growth over secondary radial growth (Lanner 1985). Consequently, the HD ratio
- is a useful predictor of assimilate partitioning among tree organs (West 1993; King 2005).
- 20 Under the assumption that stem or branch area increments are proportional to biomass
- 21 accumulation, our results indicate a shift in assimilate allocation towards branches when tree
- 22 growth is constrained by competition. Likewise, Vincent (2006) found that lower light levels

- 1 were associated with an increase in leaf life span, while King (1997) showed that the percentage
- 2 of biomass allocated to branches was higher in understory seedlings than in those growing in
- 3 large gaps. A similar concept of functional balance has also been used to explain the decrease in
- 4 shoot : root ratio when soil nutrients are a limiting factor (Génard et al. 2007). Under the
- 5 principles of teleonomy, these may be seen as adaptive responses of trees to environmental
- 6 factors, which would optimize their growth and survival probability (Lacointe 2000).

11

12

13

14

15

16

17

18

20

21

22

8 Despite large variation in annual knot growth, even among similar sized trees, the ratio of knot to

9 stem area increment (KSR) was shown to decrease systematically with tree age. Similar

ontogenetic effects have been highlighted by Wilson (1988) to describe changes in shoot : root

ratio as a plant grows. In this study, annual reconstructions of stem and branch development

suggested that high KSR values were also positively related to the number of new branches

initiated in a growth unit. While this is in agreement with the principles highlighted above, it

appears to contradict a common result of empirical branch distribution models, which is that

vigorous trees tend to initiate more branches in a given year (Maguire 1994; Mäkinen and Colin

1999; Hein et al. 2007). However, these studies typically presented models for the number of

nodal branches i.e. those forming a pseudo-whorl (Fisher and Honda 1979). Furthermore, in

models that consider both nodal and internodal branches, smaller branches (<5mm) are usually

ignored (Colin and Houllier 1991; Auty et al. 2012). An advantage of using CT scanning

technology is that all the knots were identifiable, including those that were occluded within the

stems. Furthermore, the identification of annual growth units along the stem was made easier

because it was possible to locate, with some certainty, the initiation point of branches at the

stem's pith (Duchateau et al. 2013*b*).

2

3

4

5

6

7

8

9

10

11

12

13

14

15

16

17

18

19

The relationship of knot growth to HD ratio could be clearly seen in the simulations of individual knot growth. An increase in HD ratio led to smaller but longer-lived knots, while the converse was also true. Throughout the simulation, each knot was first located at the top of the stem but its position relative to the stem's apex shifted as the tree grew in height. Therefore, in the slower growth scenario, the fact that the knot was still growing at the end of the simulation implies a slower rate of crown recession. A lower crown base in trees subject to high competition is consistent with previous results (Sprugel 2002; Valentine et al. 2013) and offers further support for Milton's Law of resource availability and allocation. Sprugel's (2002) choice of name for this principle made reference to poet John Milton's (1667) phrase, "Better to reign in hell than serve in heaven". He used this analogy to highlight the fact that although branches in light-favored conditions will tend to grow faster, a shaded branch on a shaded tree is more likely to survive and grow than a similarly-shaded branch on a dominant tree. Our model provides a time-series illustration of this principle. The vigorous growth of the knot in the first 10 to 15 years of the accelerated growth scenario suggests that the carbon budget of the branch was more positive than branches simulated in slow growth scenarios. Despite this, branch growth ceased earlier in the accelerated growth scenario. Clearly, such behaviour could not be predicted based on individual branch carbon budgets, which leads us to question the applicability of the branch autonomy principle when modelling branch growth.

20

21

## **Modelling knot development**

Previous studies have represented the dead portion of knots as a cylinder to reflect the cessation of growth (Björklund 1997; Lemieux et al. 2001; Moberg 2001). However, around 40% of knots

1 in our sample data had declining diameter profiles in the outer stem, presumably as a result of

2 branch deterioration after death. We accounted for this trend in the knot diameter model by

3 allowing negative growth predictions (Fig. 9). The inclusion of the diameter and vertical position

increments of the previous year as predictor variables allowed for smooth transitions between the

5 knot sections, which provided realistic knot shapes. Furthermore, analysis of the model residuals

showed that the models were relatively unbiased and generally accurate.

7

9

10

11

12

13

6

4

8 In the second simulation, annual predictions of knot diameter and vertical position produced

realistic reconstructions of the real knot profiles using the known insertion point, orientation and

year of occlusion of each knot. Models that can predict the vertical and azimuthal distribution of

branches within a growth unit, as well as the initial insertion angle of each branch in the main

stem, will provide even more realistic stem profiles. Even further improvements could be gained

from the addition of a self-pruning sub-model (Mäkelä and Mäkinen 2003).

14

16

17

18

19

20

21

22

23

15 Since the stem's annual rings were only partially visible on the CT images (Fig. 1), it was

necessary to interpolate tree growth from sample discs. Despite this, our results indicate that knot

development is most strongly related to stem growth during the first 25 years of growth, by

which time knots have typically reached their maximum diameter. The use of annual rings close

to the pith of the main stem (i.e. those most likely to be detected on CT images) might therefore

provide enough information to accurately predict knot growth along the entire radial profile. In

this portion of the stem, algorithms can be used for automatically detecting annual growth rings

(Jaeger et al. 1999; Longuetaud et al. 2005), which could decrease the time required for data

analysis in future studies.

2	The linear interpolation	of annual ring	width variation	between two	sample discs	was a
	1	Č				

- 3 simplification, since in reality growth rings deviate around knots (Pellicane and Franco 1994).
- 4 For this reason, the demarcation between stem and knot xylem cannot be considered as perfectly
- 5 discrete. Knot profiles were therefore extracted from the CT images by manually delineating
- 6 high density wood corresponding to a knot and the surrounding lower density stem wood.
- 7 Although the transition was generally clear enough to ensure accuracy (Fig. 1), the knot
- 8 reconstruction process produced some localized irregularities that did not reflect the true shape
- 9 of the knots. For this reason, we chose to smooth the radial profiles of each knot using a
- 10 combination of two Weibull equations, which can reproduce a wide variety of knot profiles
- 11 (Duchateau et al. 2013*a*). It is possible, however, that abrupt variations in knot shape were
- missed due to the smoothing process. The interpretation of our results on knot and stem
- allocation should therefore focus on general, long-term trends rather than on inter-annual
- variation. In fact, the long-term trends presented at the stem level should be more robust, since
- 15 they aggregate information from a large number of individual knot profiles.

16

17

# **Conclusion**

- 18 This study has provided an improved representation of the internal structure of tree stems by
- 19 linking knot development with stem growth. The use of CT scanning data allowed us to
- 20 reconstruct knot and stem ontogeny with unprecedented detail over a substantial time period. We
- 21 have found evidence for increased allocation to branches under conditions that limit the
- secondary growth of the stem, which indicates that branches are non-autonomous entities. We
- 23 have also produced a model of individual knot morphology that could provide greater precision

- 1 in the representation of knots in FSTMs, thus expanding their applicability to the wood
- 2 processing sector.

# 4 Acknowledgements

- 5 The authors are grateful to the Natural Sciences and Engineering Research Council of Canada
- 6 (NSERC) for the financial support for this project through the ForValueNet strategic research
- 7 network on forest management for value-added products. We are also grateful to Amélie
- 8 Denoncourt, Louis Gauthier, Fabien Lanteigne, Vanessa Joly, Alice Bernier Banville, Eugénie
- 9 Arsenault, and Caroline Hamelin for their assistance in collecting the samples. Two anonymous
- 10 reviewers provided helpful comments on an earlier version of the manuscript. The UMR 1092
- 11 LERFoB is supported by the French National Research Agency through the Laboratory of
- 12 Excellence ARBRE (ANR-12- LABXARBRE-01).

13

14

# Literature cited

- Abramoff MD, Magalhaes PJ, Ram SJ. 2004. Image processing with ImageJ. Biophotonics International 11: 36–43.
- Achim A, Gardiner B, Leban J, Daguitaine R. 2006. Predicting the branching properties of Sitka spruce grown in
- 17 Great Britain. New Zealand Journal of Forestry Science **36**: 246–264.
- 18 **Akaike H. 1974.** A new look at the statistical model identification. *IEEE Trans Autom Control* **19**: 716–723.
- 19 Auty D, Weiskittel AR, Achim A, Moore JR, Gardiner BA. 2012. Influence of early re-spacing on Sitka spruce
- branch structure. *Annals of Forest Science* **69**: 1–12.
- 21 Barrette J, Pothier D, Ward C. 2013. Temporal changes in stem decay and dead and sound wood volumes in the
- 22 northeastern Canadian boreal forest. Canadian Journal of Forest Research 43: 234–244.
- 23 Bates D, Maechler M, Bolker BM and Walker S. 2014. "Ime4: Linear mixed-effects models using Eigen and S4."
- 24 ArXiv e-print; submitted to Journal of Statistical Software, <URL:http://arxiv.org/abs/1406.5823>.

- Björklund L. 1997. The interior knot structure of Pinus sylvestris stems. Scandinavian Journal of Forest Research
- 2 **12**: 403–412.
- 3 Bosc A. 2000. EMILION, a tree functional-structural model: Presentation and first application to the analysis of
- 4 branch carbon balance. *Annals of Forest Science* **57**: 555–569.
- 5 Bouchard M, Pothier D, Gauthier S. 2008. Fire return intervals and tree species succession in the North Shore
- 6 region of eastern Quebec. Canadian Journal of Forest Research 38: 1621–1633.
- 7 Buksnowitz C, Hackspiel C, Hofstetter K, Muller U, Gindl W, Teischinger A, Konnerth J. 2010. Knots in trees:
- 8 strain distribution in a naturally optimised structure. *Wood Science and Technology* **44**: 389–398.
- 9 Colin F, Houllier F. 1991. Branchiness of Norway spruce in north-eastern France Modeling vertical trends in
- maximum nodal branch size. *Annales Des Sciences Forestieres* **48**: 679–693.
- 11 Colin F, Mothe F, Freyburger C, Morisset J-B, Leban J-M, Fontaine F. 2010. Tracking rameal traces in sessile
- oak trunks with X-ray computer tomography: biological bases, preliminary results and perspectives. Trees 24: 953–
- 13 967.
- 14 **Dinwoodie JM**. **2000**. *Timber: Its nature and behaviour*. Taylor & Francis.
- 15 Duchateau E, Longuetaud F, Mothe F, Ung C-H, Auty D, Achim A. 2013a. Modelling knot morphology as a
- function of external tree and branch attributes. *Can. J. For. Res.* **43**: 266–277.
- Duchateau E, Auty D, Mothe F, Achim A. 2013b. Improving branch distribution models in trees using X-ray
- 18 computed tomography. 7th International Conference on Functional-Structural Plant Models, Saariselkä, Finland.
- 19 Saariselkä, Finland. http://www.metal.fi/fspm2013/proceedings. ISBN 978-951-651-408-9
- 20 **Dutilleul P, Han LW, Beaulieu J. 2014.** How do trees grow? Response from the graphical and quantitative analyses
- of computed tomography scanning data collected on stem sections. Comptes rendus biologies 337: 391–8.
- Fisher JB, Honda H. 1979. Branch geometry and effective leaf area: a study of Terminalia-branching pattern. 1.
- Theoretical trees. American Journal of Botany **66**: 633–644.
- 24 Génard M, Dauzat J, Franck N, Lescourret F, Moitrier N, Vaast P, Vercambre G. 2007. Carbon allocation in fruit
- trees: from theory to modelling. *Trees* **22**: 269–282.
- 26 Guay R, Gagnon R, Morin H. 1992. A new automatic and interactive tree ring measurement system based on a line
- scan camera. *The Forestry Chronicle* **68**: 138–141.
- 28 Hein S, Mäkinen H, Yue CF, Kohnle U. 2007. Modelling branch characteristics of Norway spruce from wide
- spacings in Germany. Forest Ecology and Management **242**: 155–164.
- 30 Hein S, Weiskittel AR, Kohnle U. 2008. Effect of wide spacing on tree growth, branch and sapwood properties of
- 31 young Douglas-fir [Pseudotsuga menziesii (Mirb.) Franco] in south-western Germany. European Journal of Forest
- 32 Research 127: 481–493.

- Jaeger M, Leban JM, Borianne P, Chemouny S, Saint-André L. 1999. 3D stem reconstruction from CT scan
- 2 exams. From log external shape to internal structures. In: 01 IWS, ed. Connection between Silviculture and wood
- 3 quality through modelling approaches and simulation software.
- 4 King D a. 1997. Branch growth and biomass allocation in Abies amabilis saplings in contrasting light environments.
- 5 Tree physiology **17**: 251–258.
- 6 King D a. 2005. Linking tree form, allocation and growth with an allometrically explicit model. Ecological Modelling
- 7 **185**: 77–91.
- 8 Kull O, Tulva I. 2000. Modelling canopy growth and steady-state leaf area index in an aspen stand. *Annals of Forest*
- 9 Science **57**: 611–621.
- 10 Lacointe A. 2000. Carbon allocation among tree organs: A review of basic processes and representation in
- 11 functional-structural tree models. *Annals of Forest Science* **57**: 521–533.
- 12 Landsberg JJ, Waring RH. 1997. A generalised model of forest productivity using simplified concepts of radiation-
- use efficiency, carbon balance and partitioning. Forest Ecology and Management **95**: 209–228.
- Lanner RM. 1985. On the insensitivity of height growth to spacing. Forest Ecology and Management 13: 143–148.
- Lemieux H, Beaudoin M, Zhang SY. 2001. Characterization and modeling of knots in black spruce (Picea mariana)
- 16 logs. Wood and Fiber Science **33**: 465–475.
- 17 **Lemieux H, Beaudoin M, Zhang SY, Grondin F. 2002**. Improving structural lumber quality in a sample of Picea
- mariana logs sawn according to the knots. *Wood and Fiber Science* **34**: 266–275.
- Longuetaud F, Mothe F, Kerautret B, Krähenbühl A, Hory L, Leban JM, Debled-Rennesson I. 2012. Automatic
- 20 knot detection and measurements from X-ray CT images of wood: A review and validation of an improved algorithm
- 21 on softwood samples. Computers and Electronics in Agriculture **85**: 77–89.
- 22 Longuetaud F, Saint-Andre L, Leban JM. 2005. Automatic detection of annual growth units on Picea abies logs
- using optical and x-ray techniques. *Journal of Nondestructive Evaluation* **24**: 29–43.
- Maguire DA. 1994. Branch mortality and potential litterfall from Douglas-Fir trees in stands of varying density. Forest
- 25 Ecology and Management 70: 41–53.
- Mäkelä A, Mäkinen H. 2003. Generating 3D sawlogs with a process-based growth model. Forest Ecology and
- 27 *Management* **184**: 337–354.
- 28 **Mäkinen H, Colin F. 1999.** Predicting the number, death, and self-pruning of branches in Scots pine. *Canadian*
- 29 Journal of Forest Research 29: 1225–1236.
- 30 **Mäkinen H, Mäkelä A. 2003**. Predicting basal area of Scots pine branches. Forest Ecology and Management 179:
- 31 351–362.
- 32 Mathieu A, Cournede PH, Letort V, Barthelemy D, de Reffye P. 2009. A dynamic model of plant growth with
- interactions between development and functional mechanisms to study plant structural plasticity related to trophic
- 34 competition. *Annals of Botany* **103**: 1173–1186.

- 1 Milton J. 1667. Paradise Lost. Peter Parker, London, 368 p.
- 2 Mitchell KJ. 1975. Dynamics and Simulated Yieldof Douglas-fir. Forest Science: a0001–z0001.
- 3 Moberg L. 2001. Models of internal knot properties for Picea abies. Forest Ecology and Management 147: 123–138.
- 4 Moberg L, Nordmark U. 2006. Predicting lumber volume and grade recovery for Scots pine stems using tree models
- and sawmill conversion simulation. Forest Products Journal **56**: 68–74.
- 6 Mothe F. 2014. http://www6.nancy.inra.fr/foret-bois-lerfob/Zoom-sur/Outils-pour-le-traitement-d-
- 7 images/Tomographie-X/Encodage
- 8 Nikinmaa E, Hari P. 1990. A simplified carbon partitioning model for Scots pine to address the effects of altered
- 9 needle longevity and nutrient uptake on stand development. In: Dixon R, Meldahl R, RUARK G, Warren W, eds.
- 10 Process modeling of forest growth responses of environmental stress. Portland, USA: Timber Press Inc, 263–270.
- Nikinmaa E, Messier C, Sievänen R, Perttunen J, Lehtonen M. 2003. Shoot growth and crown development:
- effect of crown position in three-dimensional simulations. *Tree physiology* **23**: 129–36.
- 13 O'brien RM. 2007. A Caution Regarding Rules of Thumb for Variance Inflation Factors. Quality & Quantity 41: 673–
- 14 690.
- Pellicane PJ, Franco N. 1994. Modeling wood pole failure. Wood Science and Technology 28: 261–274.
- Pinheiro JC, Bates DM. 2009. *Mixed-effects models in S and S-PLUS*. Springer.
- 17 **Pretzsch H. 2005.** Diversity and productivity in forests: evidence from long-term experimental plots. *Forest diversity*
- 18 and function. Springer, 41–64.
- 19 R Core Team 2014. R: A language and environment for statistical computing. R Foundation for Statistical
- 20 Computing, Vienna, Austria. URL http://www.R-project.org/.
- 21 Sievänen, R., Nikinmaa, E., Nygren, P., Ozier-Lafontaine, H., Perttunen, J., Hakula, H., 2000. Components of
- functional-structural tree models. Ann. For. Sci. 57, 399–412.
- 23 Sprugel DG. 2002. When branch autonomy fails: Milton's Law of resource availability and allocation. Tree
- 24 *Physiology* **22**: 1119–1124.
- 25 **Sprugel DG, Hinckley TM**. **1988**. The branch autonomy concept. Response of trees to air pollution: The Role of
- Branch Studies. In: Winner W.E. & Phelps L.G. E, ed. *Proc. Workshop National Forest Response Program.*7–23.
- 27 Torquato LP, Auty D, Hernández RE, Duchesne I, Pothier D, Achim A. 2014. Black spruce trees from fire-origin
- stands have higher wood mechanical properties than those from older, irregular stands 1. 10: 1–10.
- 29 Valentine HT, Amateis RL, Gove JH, Mäkelä A. 2013. Crown-rise and crown-length dynamics; application to
- 30 loblolly pine. *Forestry* **86**: 371–375.
- Vincent G. 2006. Leaf life span plasticity in tropical seedlings grown under contrasting light regimes. *Annals of*
- 32 Botany 97: 245–55.

- 1 Van der Wal DW. 1985. A proposed concept of branch autonomy and non-ring production in branches of Douglas-fir
- and grand fir. (Doctoral dissertation, University of Washington).
- Ward C, Pothier D, Paré D. 2014. Do Boreal Forests Need Fire Disturbance to Maintain Productivity? Ecosystems
- 4 17: 1053–1067.
- Weiskittel AR, Hann DW, Kershaw Jr JA., Vanclay JK. 2011. Forest Growth and Yield Modeling. Chichester, UK:
- 6 John Wiley & Sons, Ltd.
- Weiskittel AR, Maguire DA, Monserud RA. 2007. Response of branch growth and mortality to silvicultural
- 8 treatments in coastal Douglas-fir plantations: Implications for predicting tree growth. Forest Ecology and
- 9 *Management* **251**: 182–194.
- West PW. 1993. Model of above-ground assimilate partitioning and growth of individual trees in even-aged forest
- 11 monoculture. *Journal of Thoeretical Biology* **161**: 369–394.
- Wilson JB. 1988. A review of evidence on the control of shoot: root ratio, in relation to models. Annals of Botany 61:
- 13 433–449.

	Age	Number of complete rings used on the analysis	Total Height (m)	Diameter at breast height (cm)	Length of the crown (m)	Number of measured knots
T01	82	14	14.02	15.4	5.04	726
T02	85	19	14.15	14.1	4.3	620
T03	86	27	15.27	15.6	4.8	819
T04	93	32	11.81	14.3	2.09	568
T05	104	45	14.22	16.3	5.32	1066
T06	106	47	20.52	22.2	8.77	1198
T07	113	48	18.2	21.4	5.82	514
T08	118	51	16.92	21.8	8.32	1121
T09	139	78	16.28	17.8	5.42	993
T10	152	84	20.8	22.4	5.25	1518
mean	107.8	68.5	16.219	18.13	5.513	914.3
sd	23.47	24.36	2.93	3.45	1.90	321.14

	Description
Tree-level variables	
DBH <sub>t</sub>	Diameter of the tree at 1.3 m at time $t$ (mm)
$Age_t$	Age of the tree at time t
$\mathrm{GU}_{\mathrm{len}}$	Length of the annual growth unit (m)
$HD_t$	Ratio of total tree height to DBH calculated for each year of growth at time t
KSR <sub>t</sub>	Ratio of total knot area increment to the stem basal area increment at time $t$
Ring-level variables	
RN	Annual ring number from the pith of the main stem at the level of each knot
$RW_t$	Annual ring width at time t (mm)
$l_{,t}$	Distance from the from the pith of the stem at time t (mm)
$\mathrm{GU}_{\mathrm{pos}}$	Relative position of the knot initiation point along the annual growth unit (varies from 0 to 1)
$H_k$	Position of the initiation point of the knot along the stem (ground level = 0) (m)
<b>Knot-level variables</b>	
$\Delta D_t$	Annual increment of the knot diameter from time t-1 to t (mm)
$D_{t}$	Predicted knot diameter at time t (mm)
$\Delta Z_{t}$	Annual increment of the vertical position of the knot from time t-1 to t (mm)

- 1 Table 3 Fixed effects parameter estimates and standard errors of the KSR model given by
- 2 equation (2) and the model for the number of new branches given by equation (3).

	•	٦
	9	٠
	ı	
	П	1

Model	Parameter	Estimate	S.E.	<i>P</i> -value
	a1	-0.3956	0.11947	<0.0001
equation (2)	a2	4.1717	0.23896	<0.0001
	a3	-0.0114	0.00169	<0.0001
	b1	1.7864	0.15040	<0.0001
	b2	0.0354	0.00934	<0.0001
equation (3)	b3	0.0153	0.00105	<0.0001
	b4	-0.0006	0.00024	<0.0001

- 1 **Table 4** Fixed effects parameter estimates and standard errors for each section of the knot
- 2 diameter model given by equation (4). Section 1: knot initiation (1 to 3 years), Section 2: growth
- 3 phase (4 to 25 years), Section 3: stabilisation and death (>25 years).

		Section 1		Section 2			Section 3		
Parameter	Estimate	S.E	<i>P</i> -value	Estimate	S.E	<i>P</i> -value	Estimate	S.E	<i>P</i> -value
c1				-0.0338	0.01127	0.0026	0.0139	0.00198	<0.0001
c2				0.5166	0.00219	<0.0001	0.9699	0.00150	<0.0001
c3	1.0144	0.00671	<0.0001	-0.0302	0.00047	<0.0001	-0.0020	0.00006	<0.0001
c4	0.3661	0.01665	<0.0001	0.1285	0.00508	<0.0001	0.0068	0.00058	<0.0001
c5							0.0002	0.00002	<0.0001
c6	0.2653	0.01055	<0.0001	0.1031	0.00094	<0.0001	0.0057	0.00053	<0.0001
c7				0.0549	0.00628	<0.0001			
c8				-0.0004	0.00011	0.0003	-0.0001	0.00002	<0.0001
c9	-0.0011	0.00029	<0.0001	-0.0004	0.00008	<0.0001	-0.0002	0.00001	<0.0001
c10							0.0006	0.00017	<0.0001

- 1 Table 5 Fixed effects parameter estimates and standard errors for each section of the knot
- 2 vertical position model given by equation (5). Section 1: typically increasing vertical position
- 3 (years 0 to 50), Section 2: typically decreasing vertical position (years > 50).

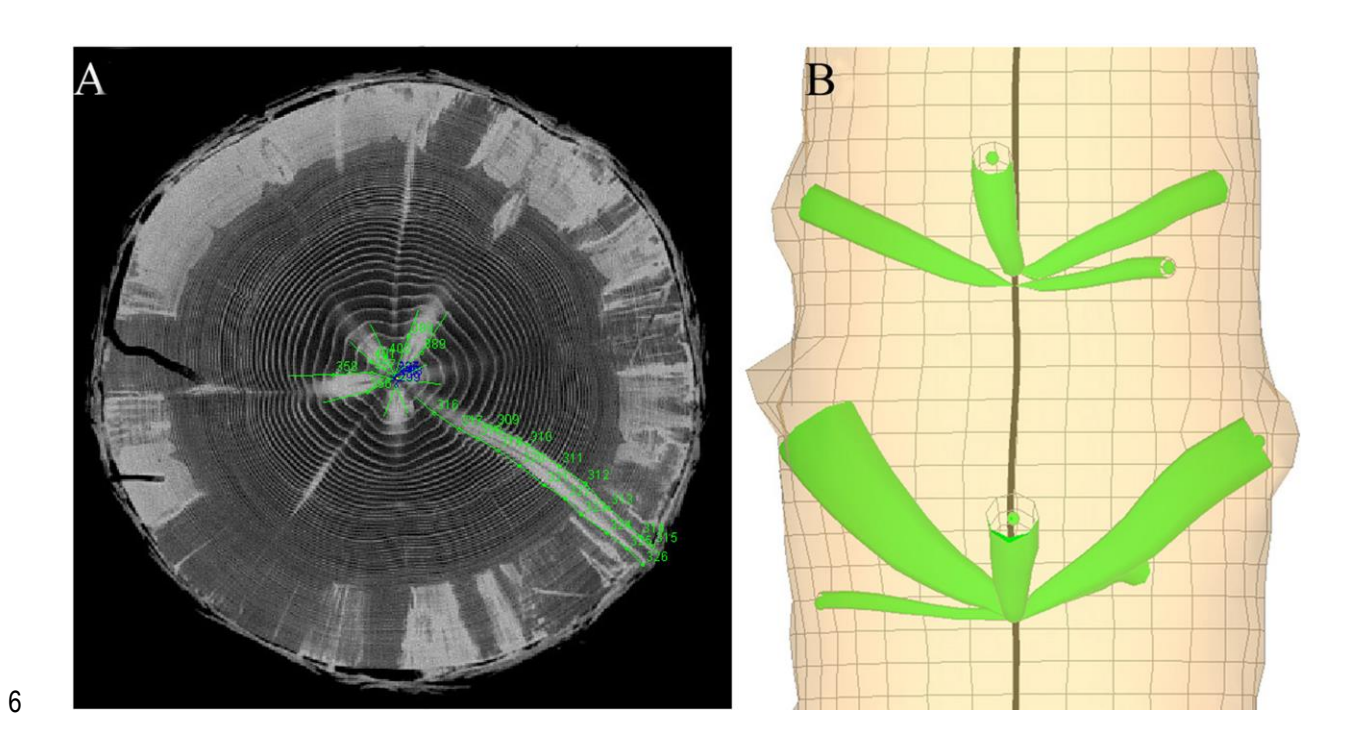
4
---

Section 1				Section 2		
Parameter	Estimate	S.E	<i>P</i> -value	Estimate	S.E	P-value
$d_1$	-0.2753	0.03019	<0.0001	0.0188	0.00447	<0.0001
$d_2$	-0.0027	0.00025	<0.0001	-0.0003	0.00014	0.0328
$d_3$	0.1864	0.00236	<0.0001	0.9719	0.00391	<0.0001
$d_4$	-0.0039	0.00012	<0.0001	0.0002	0.00004	<0.0001
$d_5$	0.1294	0.00097	<0.0001	-0.0357	0.00255	<0.0001
$d_6$	0.2498	0.00927	<0.0001	-0.0033	0.00149	0.0252
d <sub>7</sub>	0.0064	0.00211	0.0024			
$d_8$	0.0036	0.00015	< 0.0001			
$d_9$	0.0009	0.00009	<0.0001	0.0001	0.00004	0.0074

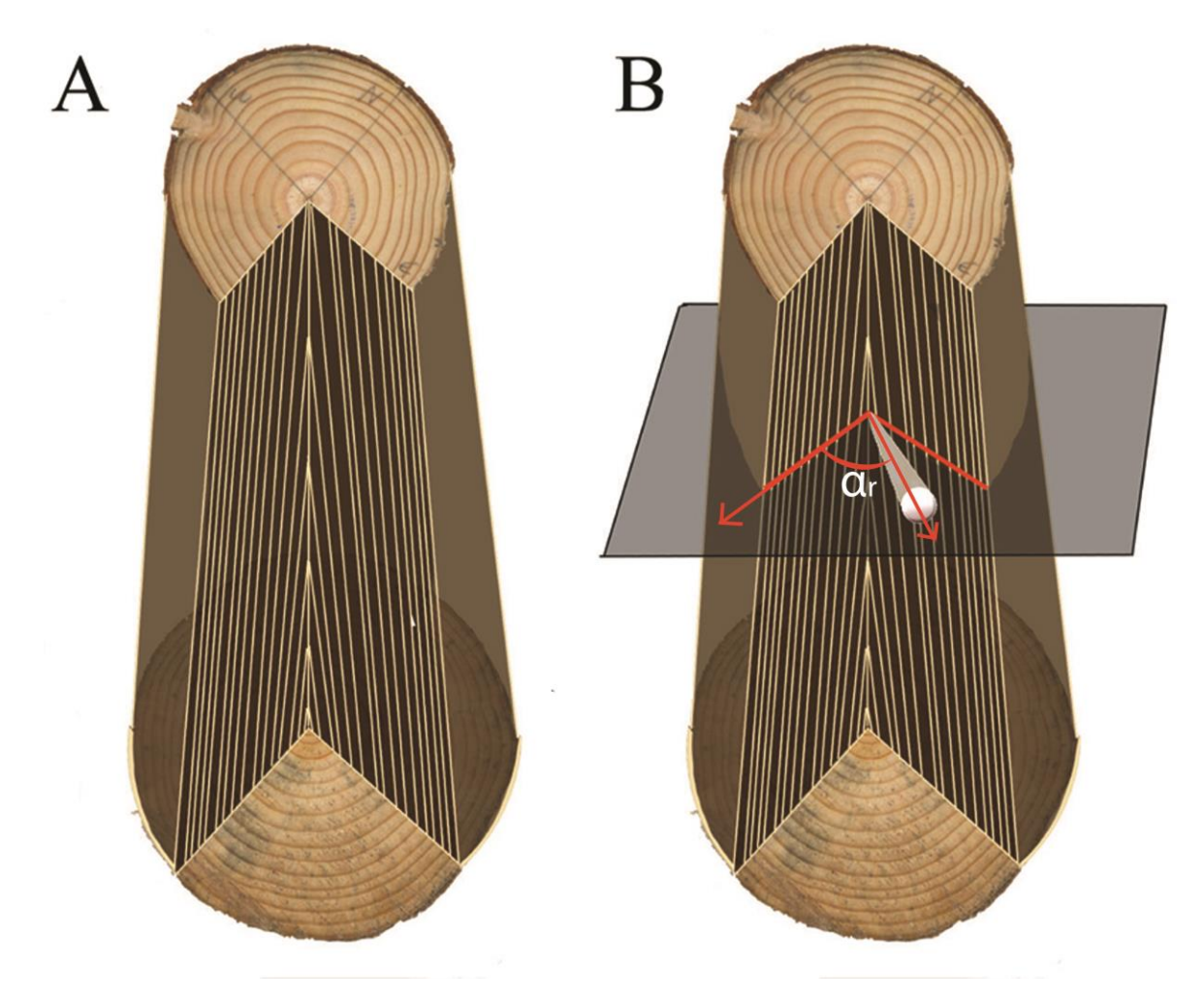
### 1 Captions for figures

2

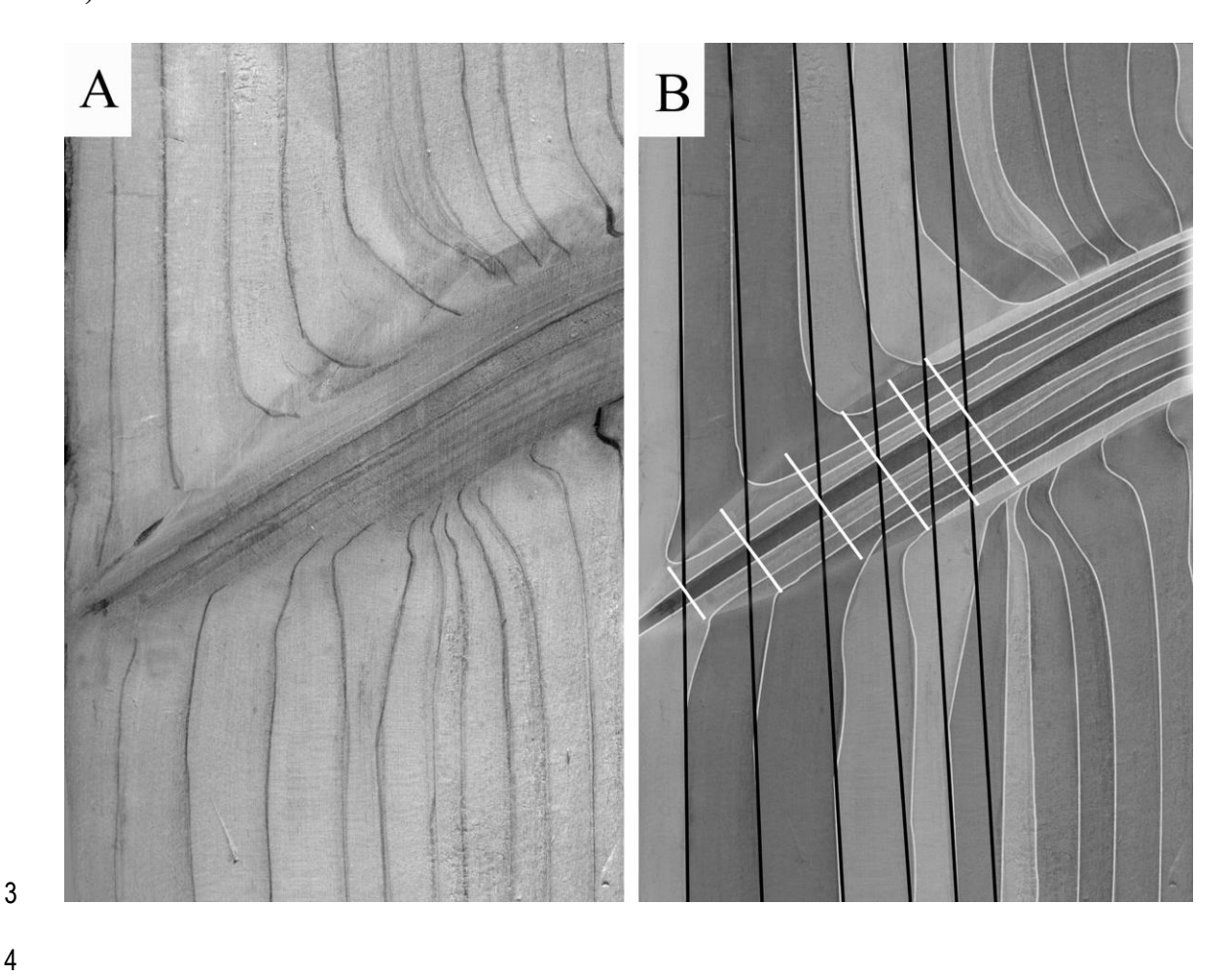
- 3 Fig. 1 The knot extraction process. A) Extraction of the position and diameter of each knot
- 4 profile on CT scanning images using the ImageJ Java plug-in 'Gourmand' and **B**) reconstruction
- 5 of the 3D geometry of each knot using the Java plug-in "Bil3D"



- 1 Fig. 2 Inferring ring width at the location of a knot A) interpolation of the rings between the two
- 2 discs to reconstruct the log and **B**) selection of the two cardinal directions bordering the knot to
- 3 reconstruct the ring widths along the knot profile.



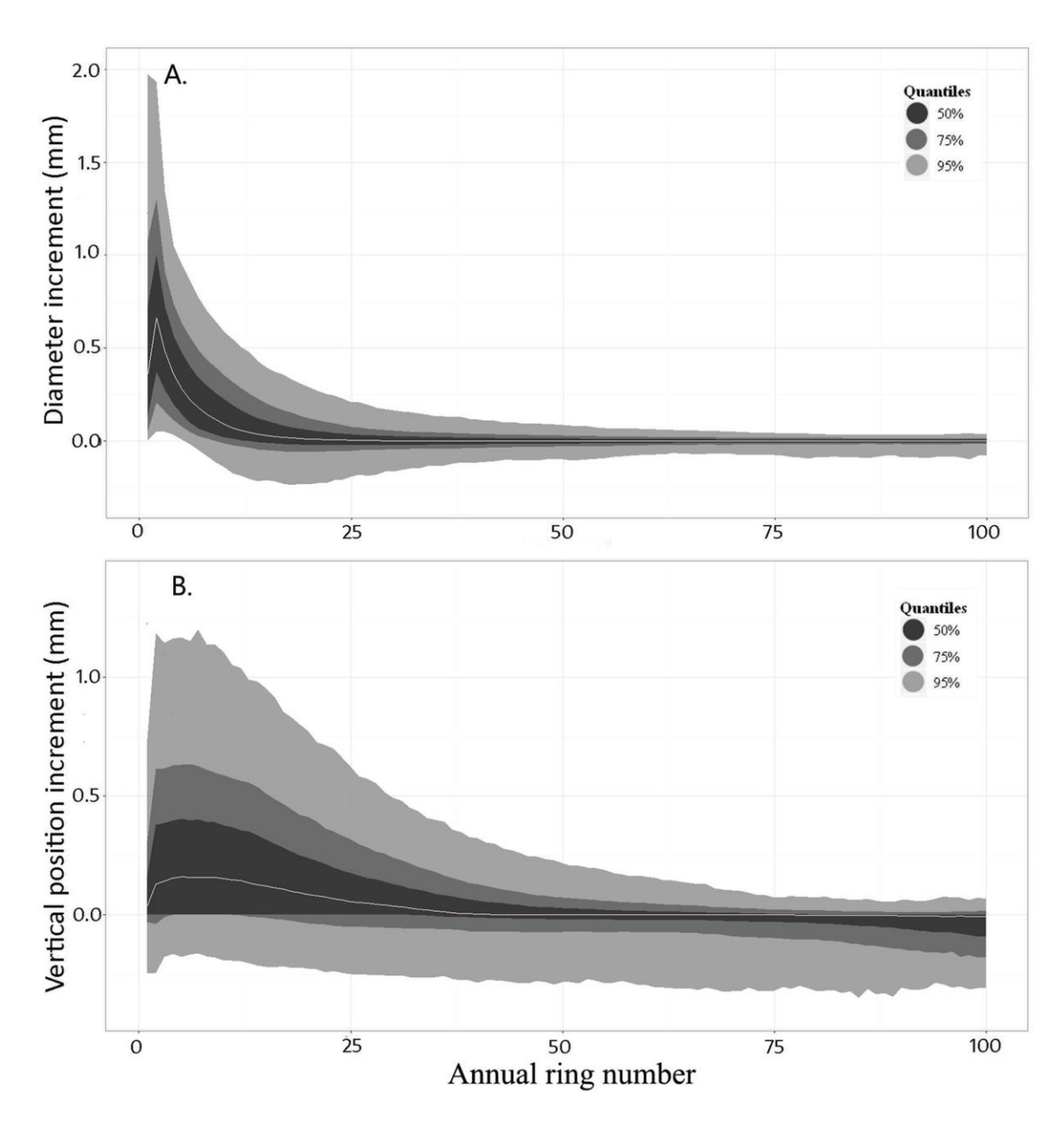
- 1 **Fig. 3** Inferring knot annual increments **A**) Example of ring width deformations around a knot;
- **B**) extraction of the annual knot data.



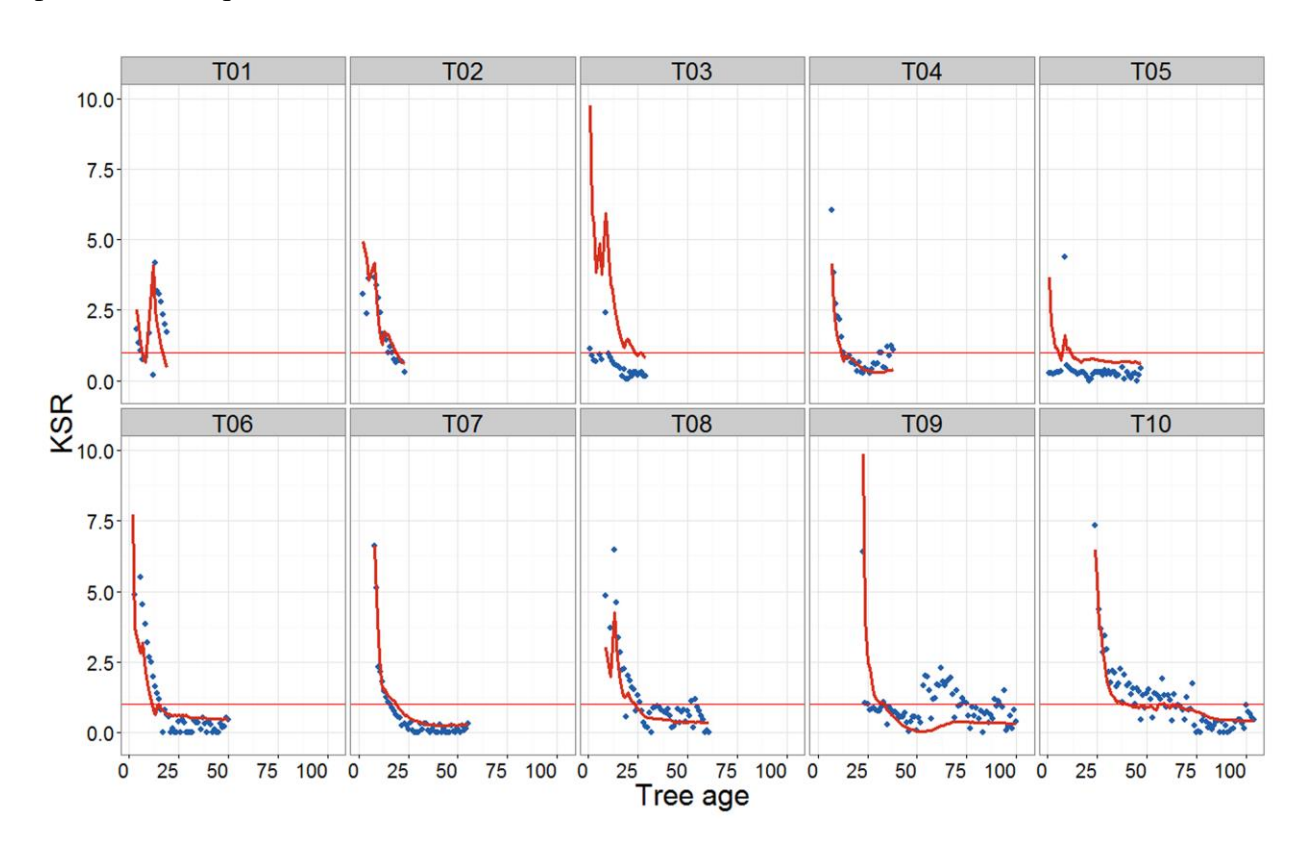
6

- 1 **Fig. 4** Distributions of annual increments in diameter  $(\Delta D_t)$  and vertical position  $(\Delta Z_t)$  of the
- 2 knot against annual ring number from the stem's pith. The grey line indicates the median of all
- 3 observations for a given ring number. Contours provide the distribution quantiles around the

### 4 median

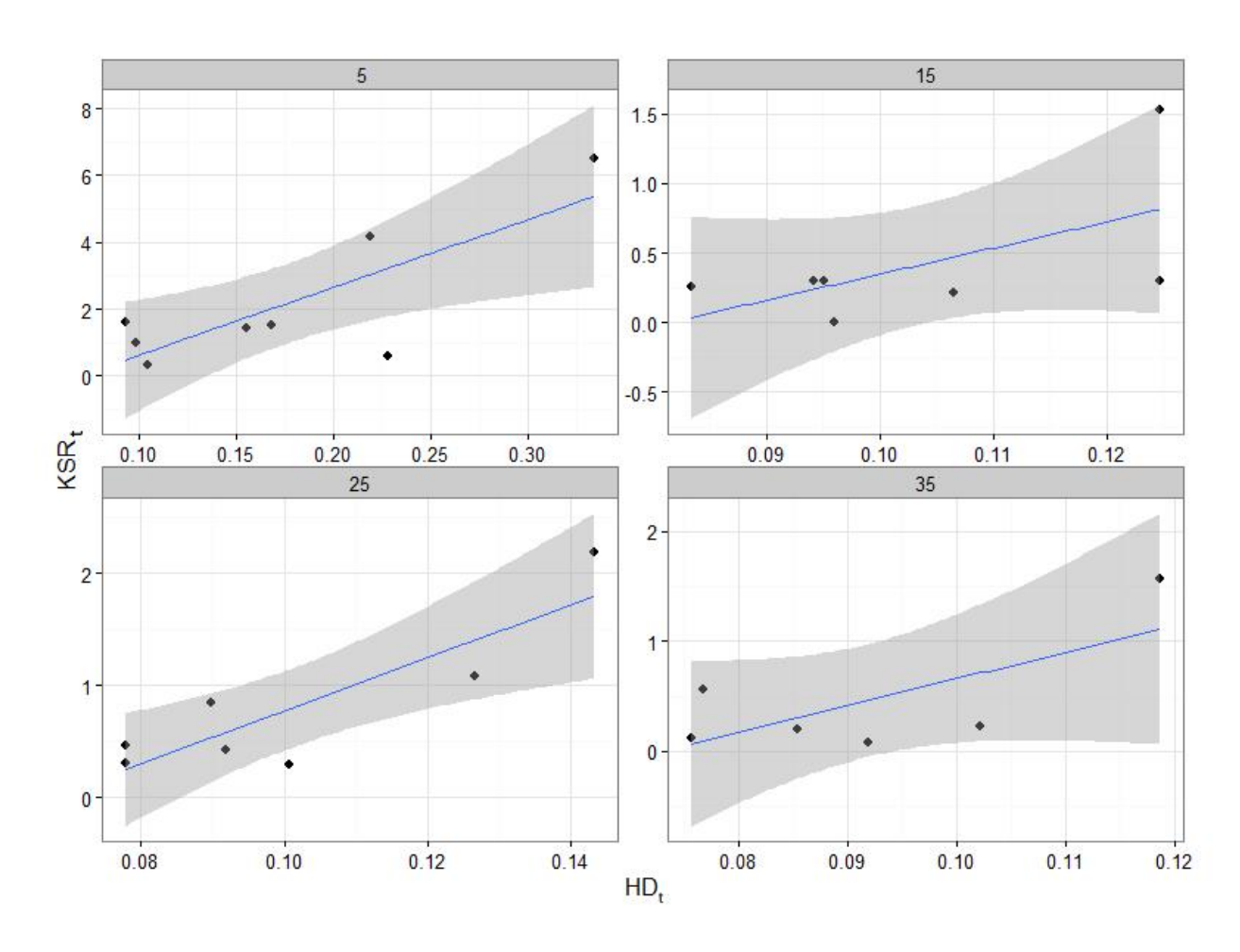


- 1 Fig. 5 Scatterplots showing the evolution of KSR (total annual knot area increment/stem
- 2 increment at 1.3 m) with tree age. Time series do not start at age 0 because HD<sub>t</sub> assessments start
- 3 when the stem has reached a height of 1.3 m. Points = observed values; red lines = model
- 4 predictions (Equation 1; Table 3)



5

- 1 Fig. 6. Scatterplots of observed KSR<sub>t</sub> vs. HD<sub>t</sub> in each sample tree for cambial ages 5, 15, 25 and
- 2 35 at breast height. The linear regressions fitted though the points show a positive correlation
- 3 between the two variables for all ages. The shaded areas represent the standard errors.



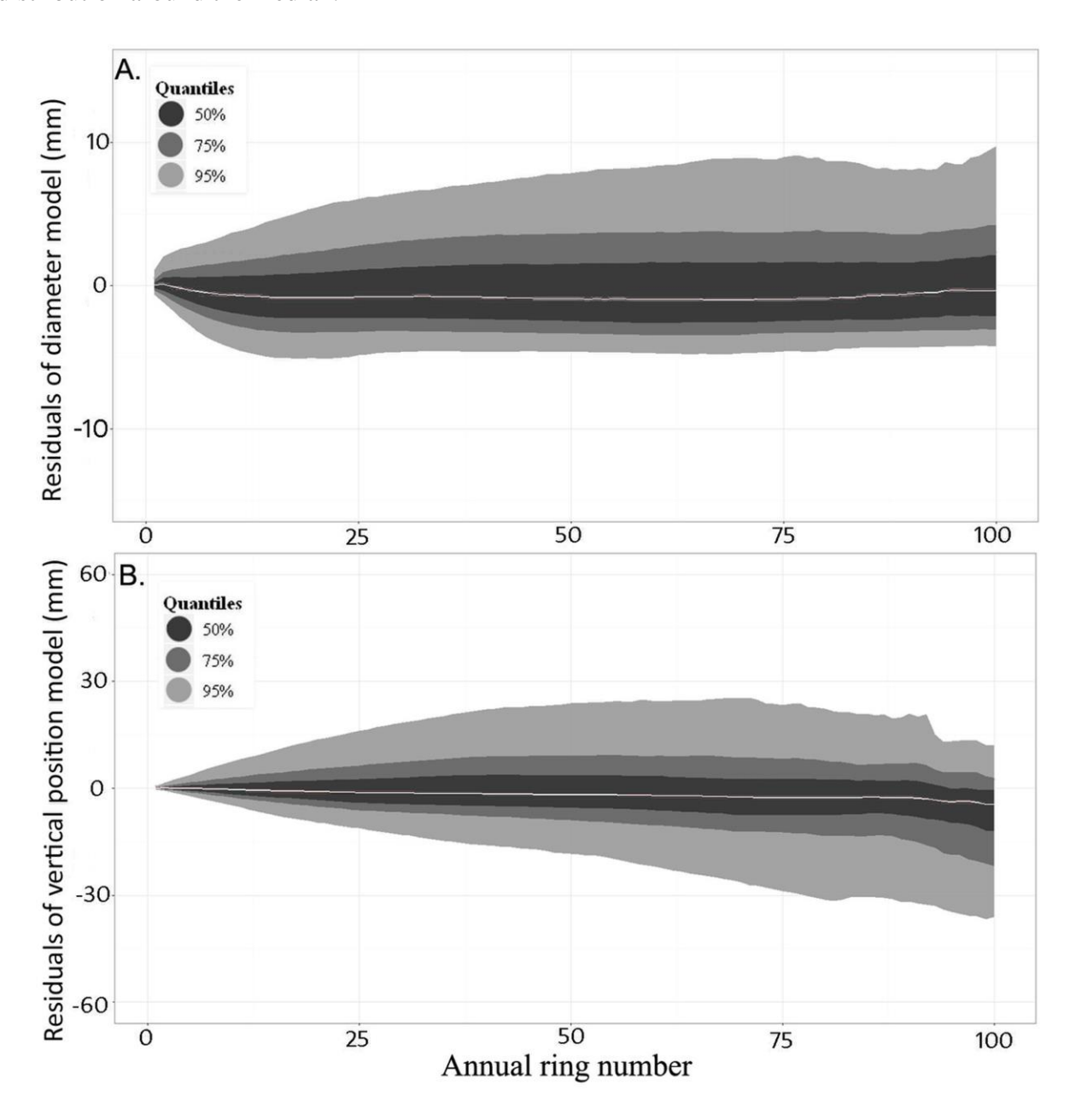
- 1 Fig. 7. 3D reconstruction of sections of two stems showing deviation of the pith related to
- 2 possible stem breakage

T01

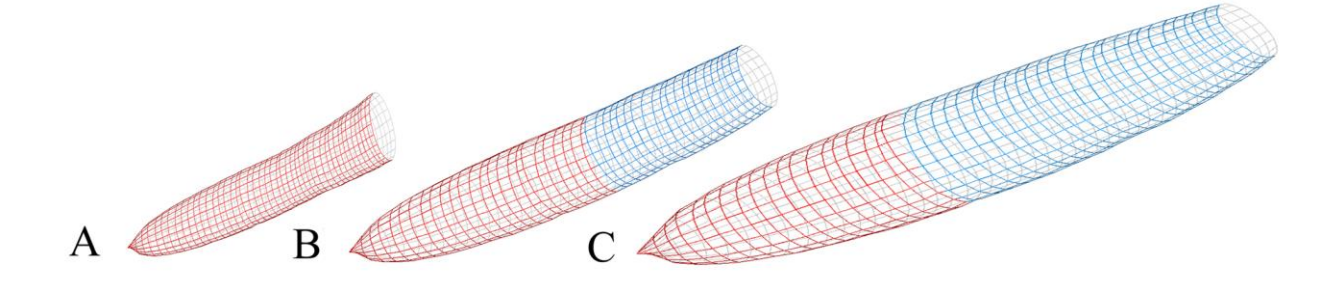
T09

3

- 1 Fig. 8 Distribution of the model residuals (sorted by quantiles) against ring number A) knot
- 2 diameter (Equation 4, Table 4) and **B**) knot vertical position (Equation 5, Table 5). The grey line
- 3 indicates the median of all observations for a given ring number. Contours provide the
- 4 distribution around the median.



- 1 Fig. 9 Simulations of a single knot from equations (4) and (5) at 6.1 m of the main stem. Stem
- 2 increments of tree T10 were used as the reference level for input parameters. A) Radial growth
- decreased by 50%; **B**) Reference level and **C**) Radial growth increased by 50%. Real height
- 4 growth from tree T10 was used for all simulations. The knot was assumed to have died when
- 5 diameter increments reached zero. Red: live section; Blue: dead section.



- 1 **Fig. 10** Reconstruction of a 1.5-m section from the base of the second log of tree T04 (i.e. at 2.5
- 2 m from the tree base). A) Real knots extracted using the CT scanning data. B) Simulated knots
- 3 using the known insertion point, azimuthal orientation around the stem, and year of occlusion.

